Amplitude- and Phase-Resolved Near-Field Mapping of Infrared Antenna Modes by Transmission-Mode Scattering-Type Near-Field Microscopy†

Martin Schnell,[‡] Aitzol Garcia-Etxarri,[§] Andreas J. Huber,[‡,∥] Kenneth B. Crozier,[⊥] Andrei Borisov,[#] Javier Aizpurua,[*,§,#] and Rainer Hillenbrand[*,‡,▽]

Nanooptics Group, CIC nanoGUNE Consolider, 20018 Donostia, San Sebastian, Spain, Centro de Física de Materiales (CSIC-UPV/EHU) and Donostia International Physics Center (DIPC), 20018 Donostia, San Sebastian, Spain, Neaspec GmbH, 82152 Martinsried, Germany, School of Engineering and Applied Sciences, Harvard University, Cambridge, Massachusetts 02138, Laboratoire des Collisions Atomiques et Moléculaires (LCAM), Université Paris Sud XI, Orsay, France, and IKERBASQUE, Basque Foundation for Science, 48011 Bilbao, Spain

Received: September 25, 2009; Revised Manuscript Received: November 28, 2009

We describe transmission-mode scattering-type near-field optical microscopy (s-SNOM) with interferometric detection. Using this technique, we map the near-field modes of infrared antennas in both amplitude and phase. The use of dielectric probing tips, higher-harmonic demodulation, and a complex-valued subtraction of residual background yields accurate near-field images of the antenna modes. We map metallic nanorods, disks, and triangles, designed for antenna resonance at mid-infrared frequencies, in good agreement with numerical calculations of the modal field distribution. Furthermore, we show that transmission-mode s-SNOM can map the *z*-component of the antenna near fields. Our results establish a basis for future near-field characterization of complex antenna structures for molecular sensing and spectroscopy.

Resonant metallic particles[1,2] and engineered micro- and nanostructures[3−9] acting as effective nanoantennas in the optical and infrared range of the spectrum allow for efficient conversion of propagating light into nanoscale confined and strongly enhanced optical fields. Nanoantennas are therefore key elements in the development of highly sensitive optical (bio)sensors[9] and light detectors,[10] optical nanolithography,[11,12] or nanoscale optical microscopy.[5,13−16]

One of the most relevant fields in which antennas have produced a striking impact is molecular spectroscopy. The capacity of nanoantennas to enhance the electromagnetic near field in their vicinity has turned these devices into adequate hosts to locate molecules and perform field-enhanced spectroscopy on them. Among the different spectroscopic options to identify and detect molecular fingerprints, vibrational spectroscopy has proven to be extremely useful for selective detection of molecular groups. Antenna-enhancing effects due to the generation of surface plasmons have been used extensively in the past decade at visible frequencies in surface-enhanced Raman scattering spectroscopy (SERS)[17−19] and, more recently, in surface-enhanced infrared spectroscopy (SEIRS),[20] in which molecular vibrations are excited directly by infrared light.[21−23] Molecular fluorescence assisted by nanoantennas[16] has also taken advantage of the enhancing capacity of nanoantennas, with additional control on the polarization and directionality of the fluorescence produced. Since the antenna−molecule interaction occurs in the near field of the antenna, a detailed understanding of the antenna properties and experimental knowledge about the near-field distribution will be essential for optimization of the antenna performance.

In addition to the magnitude of the local field enhancement, the near-field phase is an essential parameter in antenna-assisted molecular spectroscopy, as well as in a variety of coherent-control applications.[24] For example, the near-field phase plays a crucial role in antenna-assisted infrared spectroscopy because the interference between molecule and antenna near-fields can give rise to dramatic resonant effects that enhance the sensitivity and contrast of the spectral information, showing modifications of the spectral line shape of the molecules (similar to Fano resonances known from quantum physics).[22,25] Amplitude *and* phase mapping antenna modes in arbitrarily shaped objects is thus of extreme importance to understand the antenna response assisting in chemical spectroscopy. Furthermore, accessing the near fields around the nanoantennas can provide essential input for controlling and engineering the antenna response. This control is valuable in many fields of technological application, such as in optical interconnects or switchers, and can play a basic role in governing the transfer of energy,[26] the processing of quantum information,[27] and coherent-control applications. In this article, we show a way to access the near-field amplitude and phase around infrared nanoantennas, overcoming issues such as background signal and probe−antenna interactions, thus accessing directly the local fields of the antenna.

A promising tool for mapping antenna near fields is scattering-type near-field optical microscopy (s-SNOM).[2,14,28−33] This technique offers an excellent spatial resolution in the 10 nm range, independent of the wavelength, and allows for accessing both the near-field amplitude and phase. In a typical s-SNOM experiment,[14] the tip of an atomic force microscope (AFM) is illuminated with a focused laser beam, and the tip-scattered light is detected simultaneously to topography. Using metallic tips, the near-field interaction between tip and sample modifies the scattered light, yielding maps of the local dielectric sample

† Part of the "Martin Moskovits Festschrift".

* Corresponding authors. (R.H.) Phone: + 34 943 574 007. Fax: + 34 943 574 001. E-mail: r.hillenbrand@nanogune.eu. (J.A.) E-mail: aizpurua@ehu.es.

‡ CIC nanoGUNE.

§ CSIC-UPV/EHU and DIPC.

∥ Neaspec GmbH.

⊥ Harvard University.

Université Paris Sud XI.

▽ IKERBASQUE.

10.1021/jp909252z
Published on Web 01/12/2010

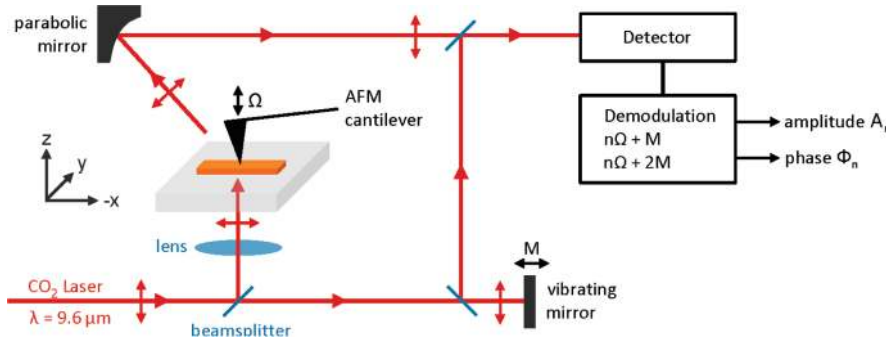

Figure 1. Setup of the transmission-mode s-SNOM with pseudoheterodyne detection.

properties with nanoscale resolution. In this particular configuration, background contributions are suppressed by vertical tip oscillation at frequency Ω and by subsequent higher-harmonic demodulation of the detector signal at $n\Omega$ with $n \geq 2$.[14] For mapping the near-field distribution of optical antennas,[2,28,29,34,35] however, the perturbation of the antenna near fields by the probing tip is recognized as a problem,[36] and certain modifications to the typical s-SNOM experiment have been introduced to avoid this perturbation, such as cross-polarization illumination schemes[31] and employing dielectric tips.[35] Here, we present transmission-mode s-SNOM[37] as an alternative illumination scheme for minimizing antenna-mode distortion by the probing tip. Compared to the cross-polarization side-illumination scheme, transmission mode offers the advantage of homogeneous antenna illumination, which prevents retardation effects[29,31] on the electromagnetic response of the sample. We also present a detailed analysis of the background in the optical images when employing dielectric tips. We show that this background can be satisfactorily removed, allowing for reproducible and quantitative mapping of the near-field distribution, especially of the near-field phase.[37] We apply this procedure to obtain the near fields in a variety of IR nanoantennas, thus showing the general applicability of the background subtraction.

Details about our setup are shown in Figure 1. The microscope is based on a tapping-mode AFM in which the tip is vertically vibrating at a frequency $\Omega = 300$ kHz and with an amplitude of 200 nm. A CO_2 laser emitting a monochromatic beam ($\lambda = 9.6$ μm, $P = 500$ mW) is focused from below through the infrared-transparent sample, illuminating both the antenna and the AFM tip. The polarization of the laser beam is chosen to be parallel to the antenna axis, thus allowing for efficient excitation of the antenna while avoiding a strong polarization of the tip. We further reduce the near-field interaction between the tip and the sample by employing dielectric Si tips (Nanosensors, type PPP-FM, HF dipped). While scanning the sample, the local optical fields in the vicinity of the antenna are scattered by the tip and collected with a parabolic mirror. Signal demodulation at higher harmonics of the tip oscillation frequency, $n\Omega$, in combination with a pseudoheterodyne interferometric detection scheme[38] yields the optical signal amplitude, A_n, and phase, θ_n.

We now apply the transmission-mode s-SNOM to image well-defined metal nanorods designed for fundamental dipolar resonance at mid-infrared frequencies. The rods (1550 nm × 230 nm × 60 nm, Figure 2b–d) were fabricated on a Si substrate by e-beam lithography and show a far-field resonance at $\lambda = 9.6$ μm wavelength.[4] For background reduction, signal demodulation needs to be done at $n = 3$ because at $n = 4$, the signal is below the noise level. Figure 2 shows the topography and infrared near-field images of three individual nanorods recorded at their dipolar resonance wavelength. Due to the characteristics of our s-SNOM setup (i.e., the polarization of the reference beam is chosen to be parallel to the tip axis), we expect the z-component of the near fields to be probed.[29,30,37] The expected dipolar pattern exhibits large near-field amplitude, A_3, at the rod extremities and a 180° phase jump at the rod center (see the calculated near-field pattern in Figure 2a). In the experimental images, however (Figure 2b–d), the near-field maps of the rods show pronounced differences. The rods c and d exhibit significant near-field amplitude, A_3, at the rod extremities, whereas the rod b exhibits a more intense near field at the left-hand side. Furthermore, the near-field phase jump, which is accompanied by a minimum in the amplitude image, appears at different positions for the three rods. The variation of the near-field images allows us to conclude that we do not obtain exact maps of the dipolar near-field oscillation.

To analyze the differences in the near-field contrast of the three rods, we recorded approach curves (Figure 2e) at three different positions along the third rod (Figure 2d), which are

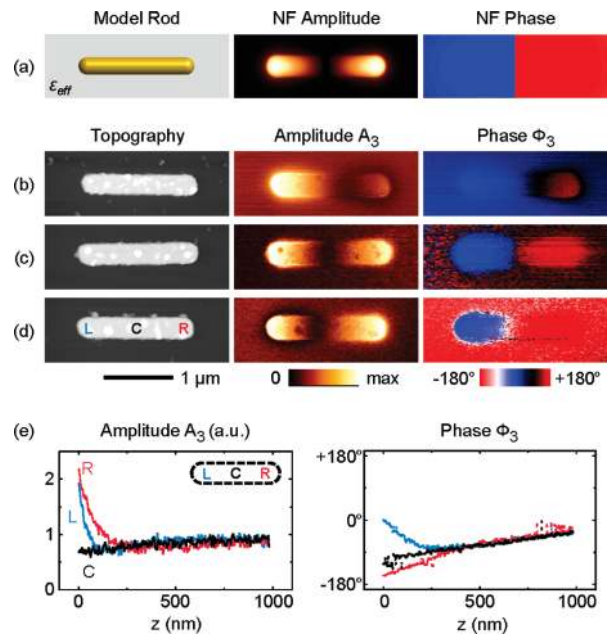

Figure 2. (a) Calculated z-component of the near fields of a resonant model rod. (b–d) Near-field modes of three individual nanorod antennas recorded at their fundamental dipolar resonance of $\lambda = 9.6$ μm wavelength. The amplitude, A_3, and phase, Φ_3, signals are shown as recorded. The polarization of the incident light is chosen parallel to the rod axis. In the phase images, the left rod end was normalized to 0°. The differences in the near-field images are due to the presence of residual background. (e) Approach curves showing the amplitude and phase signal as a function of distance, z, between the oscillating tip and the antenna surface. The approach curves were taken at the positions L, C, and R of the third nanorod (d).

marked by L, C, and R in the topography image. At the two positions L and R, we find a steep increase in the signal amplitude A_3 at tip−sample distances $z < 300$ nm, which is a typical behavior for near-field signals.[39,40] At position C, no significant changes in the amplitude and phase signals are observed at small z, thus indicating that no near-fields are detected. At distances $z > 300$ nm (i.e., beyond the near-field zone of the antennas), the three approach curves exhibit significant optical signals. This reveals the presence of a residual background contribution, $A_{3,bg}(z)$ and $\Phi_{3,bg}(z)$, in the detected s-SNOM signals A_3 and Φ_3, which is constant across the sample. Therefore, we can conclude that background contributions are not fully suppressed by signal demodulation at the higher harmonics of the tip oscillation frequency, Ω.

We now demonstrate that by subtracting this residual background contribution from s-SNOM images, we can obtain reliable near-field maps of optical antenna structures. By a complex-valued subtraction, the background-free, near-field amplitude, $s_3(x, y)$, and phase, $\varphi_3(x, y)$, can be obtained through

$$s_3(x,y)\cdot e^{i\varphi_3(x,y)} = A_3(x,y)\cdot e^{i\Phi_3(x,y)} - A_{3,bg}(z=0)\cdot e^{i\Phi_{3,bg}(z=0)} \quad (1)$$

where $A_3(x, y)$ and $\Phi_3(x, y)$ are the demodulated signals measured at the pixel position (x, y). $A_{3,bg}(z = 0)$ and $\Phi_{3,bg}(z = 0)$ are the residual background amplitude and phase in the absence of near fields obtained from approach curve C in Figure 2e. The absence of a near-field increase for the approach curve taken at the center of the rod is in agreement with the assumption that the z-component of the rods' near field is probed (the calculated z-component at the rod center is zero). We note that such mathematical near-field extraction in s-SNOM experiments[37,40] requires detection schemes where (i) amplitude and phase is mapped and (ii) where the demodulated detector signals are a linear, complex-valued sum of near-field and background contributions. Both requirements are fulfilled, for example, in heterodyne, pseudoheterodyne or phase shifting interferometric detection techniques.[37,38,40−42]

In Figure 3b−d, we show the background-free near-field images of the three rods from Figure 2b−d. After the subtraction of residual background is applied, the optical images are uniform for the three rods. We observe high near-field amplitude values at the rod extremities in all cases now, whereas the rod center and the substrate show zero near-field amplitude. The phase jump occurs at the exact center of the rod and measures 180°. Comparing the experimental background-free images with the numerical calculations, we obtain excellent agreement with the calculated z-component of the near fields on top of the antenna (Figure 3a).

Complex-valued subtraction of the background contribution also yields background-free approach curves $s_3(z)$ and $\varphi_3(z)$ (Figure 3e). The approach curves at positions L and R in this case were obtained by complex-valued subtraction of curve C:

$$s_3(z)\cdot e^{i\varphi_3(z)} = A_3(z)\cdot e^{i\Phi_3(z)} - A_{3,bg}(z)\cdot e^{i\Phi_{3,bg}(z)} \quad (2)$$

$A_3(z)$ and $\Phi_3(z)$ are the s-SNOM signals recorded for the approach curves at positions L and R, whereas the residual background $A_{3,bg}(z)$ and $\Phi_{3,bg}(z)$ are given by the approach curve taken at the rod center, C, a position chosen because there, the z-component of the near field is zero (see black curves in Figure 2e). As expected, we observe an increase in the amplitude signal $s_3(z)$ when the tip approaches the antenna positions L and R (decreasing z). Most importantly, the phase signal $\varphi_3(z)$ is nearly constant during the approach. At a fixed illumination frequency

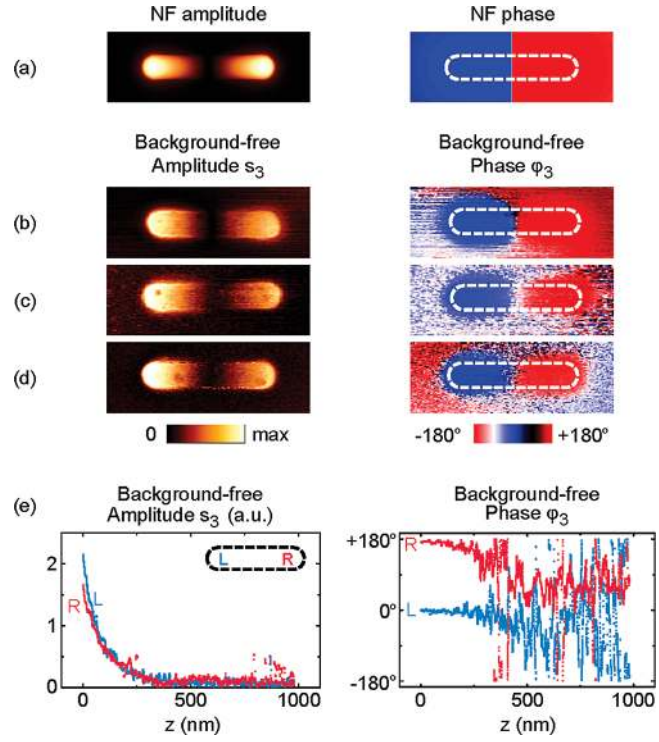

Figure 3. (a) Calculated z-component of the near fields of a resonant model rod. (b−d) Background-free amplitude and phase images of three nanorods. These images are obtained from Figure 2 after a complex-valued subtraction of residual background. The near-field patterns are exactly reproduced for the three antennas, showing the expected pattern for the fundamental dipolar oscillation mode. (e) Background-free approach curves at positions L and R on the third nanorod, obtained by complex-valued subtraction of residual background.

close to resonance (as in our experiment), any resonance shift due to tip−sample interaction would induce a significant change of phase. This, however, is not observed in Figure 3e. Thus, we can exclude tip-induced distortions of the antenna modes. Note that for strong near-field coupling between tip and antenna, we would expect spectral shifts of the antenna resonance with decreasing distance, z, analogous to near-field coupling of plasmon-resonant nanoparticles.[43−48]

In Figure 4, we compare the background-free experimental near-field images with numerical calculations (boundary element method, BEM[49,50]) of a model system consisting of a 1.55 μm-long gold nanorod of 230 nm diameter. To take into account the experimental situation in which the nanorod is situated on top of a silicon substrate with air above, the model nanorod is embedded in an effective medium of dielectric value $\varepsilon_{eff} = 6.34$. This value is chosen such that the nanorod is resonant at 9.6 μm wavelength. The x- and the z-components of the calculated near-field amplitude and phase are shown in Figure 4b. In comparison with the experimental images of the nanorod (Figure 4a), we find clear evidence that our s-SNOM probes the z-component of the near-field distribution. This behavior can be explained by the polarization of the reference beam, which is chosen parallel to the tip axis (see arrows in Figure 1). The good agreement between experiment and calculation further confirms negligible mode distortion by the probing tip, which makes s-SNOM a powerful tool for characterizing and identifying antenna near-field modes in amplitude and phase.

In Figure 4, we also demonstrate the general applicability of transmission-mode s-SNOM and the residual background subtraction for reliable near-field mapping of extended two-

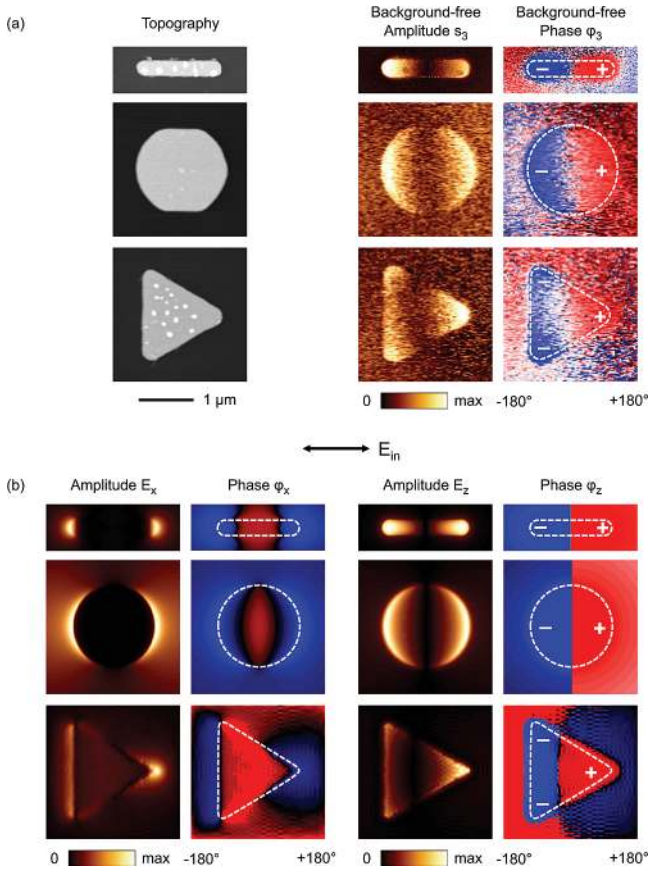

Figure 4. (a) Topography and experimental, background-free, near-field images of a rod, disk, and triangle antenna excited close to their fundamental dipolar resonance at $\lambda = 9.6$ μm wavelength. (b) Numerically calculated near-field distribution of a model rod, disk, and triangle antenna with the same dimensions as in the experiment. The maps show the *x*- and *z*-components of the electric field at a height of 51 nm above the rod surface. The boundary element method (BEM[48,49]) was applied to model the rod and the disk, assuming an effective medium of $\varepsilon_{eff} = 6.34$ to match the resonance of the experimental antennas and to take account of the Si substrate. The triangle antennas were modeled using the Lanczos pseudospectral method combined with the Lippmann−Schwinger approach.[51] The calculation of the triangle accounts explicitly for the presence of the Si substrate.

dimensional antenna structures. We image disks (1700 nm diameter × 60 nm height) and equilateral triangles (1560 nm long axis × 60 nm height), which were fabricated on a Si substrate by e-beam lithography. These infrared antennas exhibit a far-field resonance at a wavelength of about $\lambda = 10.1$ μm[4]. Near-field imaging was performed close to the resonance at $\lambda = 9.6$ μm. Residual background contributions were subtracted according to eq 1 described above. We note that the signal-to-noise ratio is better in the near-field images of the rod. We assign this to the fact that the rod was measured on resonance, whereas the disk and triangle were measured slightly off-resonance. Furthermore, the near-field images of the rod were recorded with a higher pixel resolution and with reduced scanning speed. The background-free near-field images (Figure 4a) show again excellent agreement with the *z*-component of the calculated near-field distribution (Figure 4b). For the triangle, we find in both the experimental and the calculated map a higher amplitude signal s_3 at the tip than at the base of the triangle, which can be explained by the strong field concentration at the tip. As for the rod and disk, the near fields at the tip and base of the triangle oscillate out of phase at about 180°. In contrast to the rods and disks, the phase jump on the triangle, accompanied by a minimum in the near-field amplitude, does not occur exactly in the center of the antenna but is slightly shifted toward the base of the triangle. We note that the experimental verification of such detailed near-field information is possible only by obtaining background-free near-field maps, as described here.

In conclusion, we demonstrated that transmission-mode s-SNOM employing pseudoheterodyne detection, uncoated silicon tips, and complex-valued subtraction of residual background enables reliable near-field mapping of infrared antenna modes in both amplitude and phase. The presented near-field images of infrared-resonant rods, disks, and triangles show excellent agreement with the calculated mode pattern and provide clear evidence that the *z*-component of the near-field distribution is measured. From the good agreement between experiment and theory, we can exclude mode distortion by the probing tip. This conclusion is further supported by approach curves showing that the near-field phase is independent of the probe−sample distance. Background- and distortion-free experimental near-field images promise reliable and quantitative near-field characterization of complex optical antenna structures, which can be used as hosts in molecular spectroscopy, transmitters in optical communication, and nanodevices for energy transfer.

Acknowledgment. We thank Nanosensors (Erlangen) for providing HF-etched Si tips and C. F. Quate and G. S. Kino (both Stanford University) for previous insights on the optical antennas studied in this article. We thank M. Raschke (Seattle) for stimulating discussions. Supported by the Etortek program of the Department of Industry of the Basque Government and the European FP7 project "Nanoantenna" (Health-F5-2009-241818). J.A. acknowledges the hospitality of LCAM during the elaboration of this work.

References and Notes

(1) Kreibig, U.; Vollmer, M. *Optical Properties of Metal Clusters*; Springer-Verlag: Berlin, Heidelberg, 1995.
(2) Kim, Z. H.; Leone, S. R. *Opt. Express* **2008**, *16*, 1733.
(3) Grober, R.-D.; Schoellkopf, R.-J.; Prober, D.-E. *Appl. Phys. Lett.* **1997**, *70*, 1354.
(4) Crozier, K. B.; Sundaramurthy, A.; Kino, G. S.; Quate, C. F. *J. Appl. Phys.* **2003**, *94*, 4632.
(5) Farahani, J. N.; Pohl, D. W.; Eisler, H.-J.; Hecht, B. *Phys. Rev. Lett.* **2005**, *95*, 017402.
(6) Mühlschlegel, P.; Eisler, H.-J.; Martin, O. J. F.; Hecht, B.; Pohl, D. W. *Science* **2005**, *308*, 1607.
(7) Schuck, P. J.; Fromm, D. P.; Sundaramurthy, A.; Kino, G. S.; Moerner, W. E. *Phys. Rev. Lett.* **2005**, *94*, 017402.
(8) Neubrech, F.; Kolb, T.; Lovrincic, R.; Fahsold, G.; Pucci, A.; Aizpurua, J.; Cornelius, T. W.; Toimil-Molares, M. E.; Neumann, R.; Karim, S. *Appl. Phys. Lett.* **2006**, *89*, 253104.
(9) Acimovic, S. S.; Kreuzer, M. P.; González, M. U.; Quidant, R. *ACS Nano* **2009**, *3*, 1231.
(10) Tang, L.; Kocabas, S. E.; Latif, S.; Okyay, A. K.; Ly-Gagnon, D. S.; Saraswat, K. C.; Miller, D. A. B. *Nat. Photonics* **2008**, *2*, 226.
(11) Wang, L.; Uppuluri, S. M.; Jin, E. X.; Xu, X. F. *Nano Lett.* **2006**, *6*, 361.
(12) Sundaramurthy, A.; Schuck, P. J.; Conley, N. R.; Fromm, D. P.; Kino, G. S.; Moerner, W. E. *Nano Lett.* **2006**, *6*, 355.
(13) Hartschuh, A.; Sanchez, E. J.; Xie, X. S.; Novotny, L. *Phys. Rev. Lett.* **2003**, *90*, 095503.
(14) Keilmann, F.; Hillenbrand, R. *Philos. Trans. R. Soc. London, Series A* **2004**, *362*, 787.
(15) Kalkbrenner, T.; Hakanson, U.; Schädle, A.; Burger, S.; Henkel, C.; Sandoghdar, V. *Phys. Rev. Lett.* **2005**, *95*, 200801.
(16) Taminiau, T. H.; Stefani, F. D.; Segerink, F. B.; Van Hulst, N. F. *Nat. Photonics* **2008**, *2*, 234.
(17) Moskovits, M. *Rev. Mod. Phys.* **1985**, *57*, 783.
(18) Kneipp, K.; Wang, Y.; Kneipp, H.; Perelman, L. T.; Itzkan, I.; Dasari, R. R.; Feld, M. S. *Phys. Rev. Lett.* **1997**, *78*, 1667.
(19) Nie, S.; Emory, S. R. *Science* **1997**, *275*, 1102.
(20) Aroca, R. F.; Ross, D. J.; Domingo, C. *Appl. Spectrosc.* **2004**, *58*, 324A.

(21) Le, F.; Brandl, D. W.; Urzhumov, Y. A.; Wang, H.; Kundu, J.; Halas, N. J.; Aizpurua, J.; Nordlander, P. *ACS Nano* **2008**, *2*, 707.
(22) Neubrech, F.; Pucci, A.; Cornelius, T. W.; Karim, S.; Garcia-Etxarri, A.; Aizpurua, J. *Phys. Rev. Lett.* **2008**, *101*, 157403.
(23) Kundu, J.; Le, F.; Nordlander, P.; Halas, N. J. *Chem. Phys. Lett.* **2008**, *452*, 115.
(24) Stockmann, M. I.; Faleev, S. V.; Bergmann, D. J. *Phys. Rev. Lett.* **2002**, *88*, 67402.
(25) Aizpurua, J.; Taubner, T.; de Abajo, F. J.; Brehm, M.; Hillenbrand, R. *Opt. Express* **2008**, *16*, 1529.
(26) Govorov, A. O.; Bryant, G. W.; Zhang, W.; Skeini, T.; Lee, J.; Kotov, N. A.; Slocik, J. M.; Naik, R. R. *Nano Lett.* **2006**, *6*, 984.
(27) Chang, D. E.; Sorensen, A. S.; Demler, E. A.; Lukin, M. D. *Nat. Phys.* **2007**, *3*, 807.
(28) Hillenbrand, R.; Keilmann, F.; Hanarp, P.; Sutherland, D. S.; Aizpurua, J. *Appl. Phys. Lett.* **2003**, *83*, 368.
(29) Esteban, R.; Vogelgesang, R.; Dorfmüller, J.; Dmitriev, A.; Rockstuhl, C.; Etrich, C.; Kern, K. *Nano Lett.* **2008**, *8*, 3155.
(30) Olmon, R. L.; Krenz, P. M.; Jones, A. C.; Boreman, G. D.; Raschke, M. B. *Opt. Express* **2008**, *16*, 20295.
(31) Dorfmüller, J.; Vogelgesang, R.; Weitz, R. T.; Rockstuhl, C.; Etrich, C.; Pertsch, T.; Lederer, F.; Kern, K. *Nano Lett.* **2009**, *9*, 2372.
(32) Jones, A. C.; Olmon, R. L.; Skrabalak, S. E.; Wiley, B. J.; Xia, Y. N.; Raschke, M. B. *Nano Lett.* **2009**, *9*, 2553.
(33) Kim, D.-S.; Heo, J.; Ahn, S.-H.; Han, S. W.; Yun, W. S.; Kim, Z. H. *Nano Lett.* **2009**, *9*, 3619.
(34) Hillenbrand, R.; Keilmann, F. *Appl. Phys. B: Laser Opt.* **2001**, *73*, 239.
(35) Rang, M.; Jones, A. C.; Zhou, F.; Li, Z.-Y.; Wiley, B. J.; Xia, Y.; Raschke, M. B. *Nano Lett.* **2008**, *8*, 3357.
(36) Garcia-Etxarri, A.; Romero, I.; García de Abajo, F. J.; Hillenbrand, R.; Aizpurua, J. *Phys. Rev. B: Condens. Matter Mater. Phys.* **2009**, *79*, 125439.
(37) Schnell, M.; Garcia Etxarri, A.; Huber, A. J.; Crozier, K. B.; Aizpurua, J.; Hillenbrand, R. *Nat. Photonics* **2009**, *3*, 287.
(38) Ocelic, N.; Huber, A.; Hillenbrand, R. *Appl. Phys. Lett.* **2006**, *89*, 101124.
(39) Hillenbrand, R.; Keilmann, F. *Appl. Phys. Lett.* **2002**, *80*, 25.
(40) Hillenbrand, R.; Keilmann, F. *Phys. Rev. Lett.* **2000**, *85*, 3029.
(41) Deutsch, B.; Hillenbrand, R.; Novotny, L. *Nano Lett.* DOI: 10.1021/nl9037505.
(42) Deutsch, B.; Hillenbrand, R.; Novotny, L. *Opt. Expr.* **2008**, *16*, 494.
(43) Xu, H.; Aizpurua, J.; Käll, M.; Apell, P. *Phys. Rev. E* **2000**, *62*, 4318.
(44) Rechberger, W.; Hohenau, A.; Leitner, A.; Krenn, J. R.; Lamprecht, B.; Aussenegg, F. R. *Opt. Commun.* **2003**, *220*, 137.
(45) Romero, I.; Aizpurua, J.; Bryant, G. W.; de Abajo, F. J. G. *Opt. Express* **2006**, *14*, 9988.
(46) Atay, T.; Song, J. H.; Nurmikko, A. V. *Nano Lett.* **2004**, *4*, 1627.
(47) Lassiter, J. B.; Aizpurua, J.; Hernandez, L. I.; Brandl, D. W.; Romero, I.; Lal, S.; Hafner, J. H.; Nordlander, P.; Halas, N. J. *Nano Lett.* **2008**, *8*, 1212.
(48) Nordlander, P.; Oubre, C.; Prodan, E.; Li, K.; Stockman, M. I. *Nano Lett.* **2004**, *4*, 899.
(49) Garcia de Abajo, F. J.; Howie, A. *Phys. Rev. Lett.* **1998**, *80*, 5180.
(50) Garcia de Abajo, F. J.; Howie, A. *Phys. Rev. B* **2002**, *65*, 115418.
(51) Borisov, A. G.; Shabanov, S. V. *J. Comput. Phys.* **2005**, *209*, 643.

JP909252Z